Journal of Computational Applied Mechanics 2024 , 55 (2): 184-200

DOI: 10.22059/JCAMECH.2024.371464.947

RESEARCH PAPER

Efficient Kinematic model for Stability Analysis of Imperfect Functionally Graded Sandwich Plates with Ceramic middle layer and Varied Boundary Edges

Tamrabet Abdelkader [a, b], Chitour Mourad [c], Nimer Ali Alselami [d], Abderahmane Menasria [e, f], Belgacem Mamen [e, f, g], Abdelhakim Bouhadra [e, f,*]

[a] *Department of Civil Engineering, Faculty of Technology, University of Ferhat Abbas, Setif 19137, Algeria.*
[b] *Research Unit of Emerging Materials, University of Ferhat Abbas, Setif 19137, Algeria.*
[c] *Department of Mechanical Engineering, Faculty of Science and Technology, Abbes Laghrour University, Khenchela 40000, Algeria.*
[d] *Civil Engineering Department, College of Engineering, Jazan University, Jazan 114, Saudi Arabia.*
[e] *Department of Civil Engineering, Faculty of Science and Technology, Abbes Laghrour University, Khenchela 40000, Algeria.*
[f] *Material and Hydrology Laboratory, Civil Engineering Department, Faculty of Technology, Djillali Liabes University, Sidi Bel Abbes 22000, Algeria.*
[g] *ICOSI Lab, Faculty of Science and Technology, Abbes Laghrour University, Khenchela 40000, Algeria.*

Abstract

The present paper introduces an efficient higher-order theory to analyze the stability behavior of porous functionally graded sandwich plates (FGSPs) resting on various boundary conditions. The FG sandwich plate comprises two porous FG layers, face sheets, and a ceramic core. The material properties in the FGM layers are assumed to change across the thickness direction according to the power-law distribution. To satisfy the requirement of transverse shear stresses vanishing at the top and bottom surfaces of the FGSP, a trigonometric shear deformation theory containing four variables in the displacement field with indeterminate integral terms is used, and the principle of virtual work is applied to describe the governing equation than it solved by Navier solution method for simply supported boundaries. However, an analytical solution for FGSPs under different boundary conditions is obtained by employing a new shape function, and numerical results are presented. Furthermore, validation results show an excellent agreement between the proposed theory and those given in the literature. In contrast, the influence of several geometric and mechanical parameters, such as power-law index, side-to-thickness, aspect ratio, porosity distribution, various boundary conditions, loading type, and different scheme configurations on the critical buckling, is demonstrated in the details used in a parametric study.

Keywords: Buckling analysis, functionally graded sandwich plates, porosity, higher-order theory, boundary conditions;

* Corresponding author. Tel.: +213-66-905-8481; fax: +00213-32-331-235
E-mail address: abdelhakim.bouhadra@univ-khenchela.dz

1. Introduction

Developing composite materials has achieved high levels of resistance, durability, and lightweight. According to the critical elastic deformation at the interfaces, the main drawback of convenAtional laminates is the concentration of stress between the layers and the propagation of cracks. Functionally graded materials are a new class of composite materials with specific characteristics that eliminate the weakness and the concertation stress in the traditional composite, specifically under high thermal loads. FGM presents continuous materials between two different constituents, ceramic and metal, to combine two essential properties, ceramic with thermal resistance and metal to resist under mechanical strength [1-3]. FGMs are an interesting material for different fields, including thermal and mechanical systems such as fiber-reinforced polymer in civil engineering to reinforce the concert, especially in bridges because the FRP materials increase corrosion resistance, aerospace applications to provide a high thermal barrier coating, spacecraft structures, diesel, and turbine machine, as well as the FGM has a significant role in the development of medical industries especially dental area [4, 5].

Sandwich structures are another important model designed in three layers, two face sheets in the top and bottom combined core layer; in most cases, the face and the core material are different, so the interface problem is so significant here. Hence, the key to minimizing the concentration stress is to use a smooth gradient between the two layers; the FGMs are considered in sandwich manufacturing [6].

As FGMs become more interesting materials, different plate and beam theories have a preference to study the FGM structures response; the theory in the plate can be regarded as an extension of the beam theory; on the other hand, the Euler-Bernoulli and Timoshenko beam theories both have its counterpart in Classical Love-Kirchhof plate theory and the first-order shear deformation theory. Therefore, the most straightforward theory is the classical plate theory; in the case of pure bending, the plane perpendicular to the mid-plane retains its planarity and perpendicular even after undergoing bending. While it is less accurate and needs to pay more attention to the effect of transverse stresses, it yields precise results only for thin plates [7-9]. The next plate theory in the hierarchy of refined theories is the first-order shear deformation theory (FSDT), another theory that extends the kinematics of the classical plate theory by including a gross transverse shear deformation in its kinematic assumptions. However, FSDT does not satisfy the stress-free boundary conditions on the surfaces of the plate and requires an arbitrary shear correction factor [10-13]. Furthermore, the limitation of CPT and FSDT led to the development of HSDT; the HSDT used polynomial shape functions or nonpolynomial shape functions to avoid the use of correction factor in FSDT and to develop a hypothesis more realistic from the ones of love-Kirchhoff. The HSDT introduces additional variables that are often difficult to interpret in physical terms[14].

So far, the studies on the Analysis of FG structures (beam, plate, and shell) have received too much attention from existing literature. Various theories have been developed to provide more helpful analysis methods with lower computational costs. Furthermore, some studies have been carried out on the Bending analysis of FG structures [15-18], thermal and mechanical buckling[19-24], and free and forced vibration behavior under impact loading[25-32]

Research on functionally graded sandwich structures and their mechanical behavior has been ongoing for many years. FGMs have shown great potential in eliminating stress concentration problems in sandwich structures, and various plate theories have been used to study their behavior. With continued research, it is expected that the development and application of functionally graded sandwich structures will continue to grow.

This article presents an efficient higher-order theory for the buckling analysis of porous FGSPs with varied boundary conditions. The approach considers the variation of material properties across the thickness of the FGSP, along with the effect of porosity. The analytical solutions for the functionally graded sandwich plate (FGSP) under different boundary conditions have been derived using a novel shape function. They are showcased and examined in the findings. The findings of this study can be used in designing lightweight and high-strength structures using FG sandwich plates. Numerical results are presented to validate the theory's accuracy by comparing it with other studies, and a parametric analytic study shows the influence of various parameters on the FGSP's critical buckling load, which are illustrated in detail.

2. Structure

Consider a FGSP composed of three layers, as shown in (Figure 1). The x, y, and z coordinates are taken according to the length, width, and thickness, respectively. The intermediate layer is homogeneous and consists of a purely ceramic material.

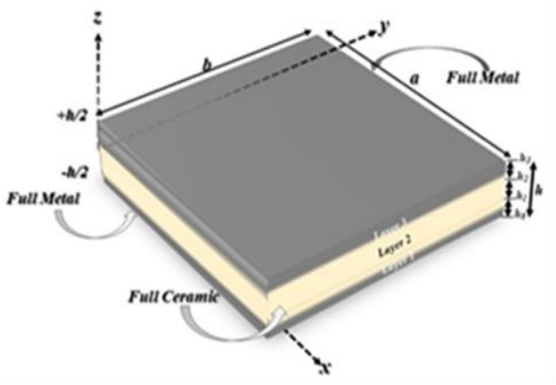

Figure 1. Geometry and coordinates of FG sandwich plates.

The material properties vary smoothly and continuously across the thickness of the FGSP and obey the following power-law distribution defined by[33]:

$$P^{(n)}(z) = P_m + (P_c - P_m)V^{(n)}(z) \tag{1}$$

With the consideration of the porosity effect[34]:

$$P^{(n)}(z) = P_m + (P_c - P_m)V^{(n)}(z) - \frac{\zeta}{2}(P_c + P_m) \tag{02}$$

Where P represents the effective material property such as E, υ, ρ; subscripts c and m denote the ceramic and metal phases, respectively; ζ denotes the porosity coefficient (ζ <1), and V is the volume fraction of layer defined by[35, 36]:

$$\begin{aligned} V^{(1)}(z) &= \left(\frac{z-h_0}{h_1-h_0}\right)^k \qquad h_0 \le z \le h_1 \\ V^{(2)}(z) &= 1 \qquad\qquad\qquad h_1 \le z \le h_2 \\ V^{(3)}(z) &= \left(\frac{z-h_3}{h_2-h_3}\right)^k \qquad h_2 \le z \le h_3 \end{aligned} \tag{3}$$

2.1. Kinematic and constitutive relations

The displacement field of the present trigonometric shear deformation theory and satisfying the conditions of transverse shear stresses vanishing at the (face sheets) top and bottom surfaces of the FGSP without including shear correction factors is of the form[29]:

$$\begin{aligned} u(x,y,z) &= u_0(x,y) - z\frac{\partial w_0}{\partial x} + k_1 f(z)\int \theta dx \\ v(x,y,z) &= v_0(x,y) - z\frac{\partial w_0}{\partial y} + k_2 f(z)\int \theta dy \\ w(x,y,z) &= w_0(x,y) \end{aligned} \tag{4}$$

Where u_0, v_0, w_0 and θ represent the unknown displacements of the mid-plane and rotations of normal to mid-plane of the FGSP. k_1 and k_2 are the constants depending on the geometry. The undetermined integrals presented in the previous equations are solved by using Navier's type solution and can be declared as:

$$u(x,y,z)=u_0(x,y)-z\frac{\partial w_0}{\partial x}+k_1 A\, f(z)\frac{\partial \theta}{\partial x}$$
$$v(x,y,z)=v_0(x,y)-z\frac{\partial w_0}{\partial y}+k_2 B\, f(z)\frac{\partial \theta}{\partial y} \tag{5}$$
$$w(x,y,z)=w_0(x,y)$$

And

$$k_1=\lambda^2,\qquad k_2=\mu^2,\quad A=-\frac{1}{\lambda^2},\quad B=-\frac{1}{\mu^2} \tag{6a}$$

Where:

$$\lambda=\frac{m\pi}{a},\qquad \mu=\frac{n\pi}{b} \tag{6b}$$

In the present study, The new shape function $f(z)$ is proposed by[37] as follows:

$$f(z)=\sin\left(\frac{z}{h}-\frac{4z^3}{3h^2}\right) \tag{7}$$

Where:

$$g(z)=\frac{df(z)}{dz}$$

Based on the small-strain elasticity theory, the deformations associated with the displacements are given as follows:

$$\begin{aligned}
\varepsilon_{xx}&=\varepsilon_{xx}^0+z\varepsilon_{xx}^1+f(z)\varepsilon_{xx}^2\\
\varepsilon_{yy}&=\varepsilon_{yy}^0+z\varepsilon_{yy}^1+f(z)\varepsilon_{yy}^2\\
\gamma_{xy}&=\gamma_{xy}^0+z\gamma_{xy}^1+f(z)\gamma_{xy}^2\\
\gamma_{yz}&=\frac{\partial f(z)}{\partial z}\gamma_{yz}^0\\
\gamma_{xz}&=\frac{\partial f(z)}{\partial z}\gamma_{xz}^0
\end{aligned} \tag{8}$$

Where:

$$\begin{Bmatrix}\varepsilon_{xx}^0\\ \varepsilon_{yy}^0\\ \gamma_{xy}^0\end{Bmatrix}=\begin{Bmatrix}\dfrac{\partial u_0}{\partial x}\\ \dfrac{\partial v_0}{\partial x}\\ \dfrac{\partial u_0}{\partial y}+\dfrac{\partial v_0}{\partial x}\end{Bmatrix},\quad \begin{Bmatrix}\varepsilon_{xx}^1\\ \varepsilon_{yy}^1\\ \varepsilon_{xy}^1\end{Bmatrix}=\begin{Bmatrix}-\dfrac{\partial^2 w_0}{\partial x^2}\\ -\dfrac{\partial^2 w_0}{\partial y^2}\\ -2\dfrac{\partial^2 w_0}{\partial x\partial y}\end{Bmatrix} \tag{9a}$$

$$\begin{Bmatrix}\varepsilon_{xx}^2\\ \varepsilon_{yy}^2\\ \varepsilon_{xy}^2\end{Bmatrix}=\begin{Bmatrix} k_1A\dfrac{\partial^2\theta}{\partial x^2}\\ k_2B\dfrac{\partial^2\theta}{\partial y^2}\\ (k_1A+k_2A)\dfrac{\partial^2\theta}{\partial x\partial y}\end{Bmatrix},\quad \begin{Bmatrix}\gamma_{xz}^0\\ \gamma_{yz}^0\end{Bmatrix}=\begin{Bmatrix} k_1A\dfrac{\partial\theta}{\partial x}+\dfrac{\partial\varphi_z}{\partial x}\\ k_2B\dfrac{\partial\theta}{\partial y}+\dfrac{\partial\varphi_z}{\partial y}\end{Bmatrix} \tag{9b}$$

For the n[th] layer, the linear constitutive relations of FGSP are given as:

$$\begin{Bmatrix}\sigma_{xx}\\ \sigma_{yy}\\ \tau_{xz}\\ \tau_{yz}\\ \tau_{xy}\end{Bmatrix}^{(n)}=\begin{bmatrix} C_{11} & C_{12} & 0 & 0 & 0\\ C_{12} & C_{11} & 0 & 0 & 0\\ 0 & 0 & C_{44} & 0 & 0\\ 0 & 0 & 0 & C_{55} & 0\\ 0 & 0 & 0 & 0 & C_{66}\end{bmatrix}^{(n)}\begin{Bmatrix}\varepsilon_{xx}\\ \varepsilon_{yy}\\ \gamma_{xz}\\ \gamma_{yz}\\ \gamma_{xy}\end{Bmatrix}^{(n)} \tag{10}$$

C_{ij} in terms of engineering constants depend on the normal strain:

- Case of 2D shear deformation, then C_{ij} are:

$$\begin{aligned} C_{11}^{(n)}&=C_{22}^{(n)}=\frac{E^{(n)}(z)}{1-(\nu^{(n)})^2}\\ C_{12}^{(n)}&=\nu^{(n)}C_{11}^{(n)}\\ C_{44}^{(n)}&=C_{55}^{(n)}=C_{66}^{(n)}=\frac{E^{(n)}(z)}{2(1+\nu^{(n)})}\end{aligned} \tag{11}$$

2.2. Stability equations

Applied the principle of virtual work and based on the adjacent equilibrium criterion, the stability equations are obtained:

$$\begin{aligned}&\int_V\left[\sigma_{xx}\,\delta\varepsilon_{xx}+\sigma_{yy}\,\delta\varepsilon_{yy}+\tau_{xy}\,\delta\gamma_{xy}+\tau_{yz}\,\delta\gamma_{yz}+\tau_{xz}\,\delta\gamma_{xz}\right]dV\\ &+\int_\Omega\left[\bar N_{xx}^0\frac{\partial w_0}{\partial x}\frac{\partial\delta w_0}{\partial x}+\bar N_{yy}^0\frac{\partial w_0}{\partial y}\frac{\partial\delta w_0}{\partial y}+\bar N_{xy}^0\frac{\partial w_0}{\partial x}\frac{\partial\delta w_0}{\partial y}\right]d\Omega=0\end{aligned} \tag{12}$$

By substituting equation. (8) into equation. (10) and the resulting equation into the equation. (12). Then, integrating through the thickness of the FGSP, equation (12) can be rewritten in the form:

$$\begin{aligned}&\int_\Omega\left[\begin{aligned}&N_{xx}^1\,\delta\varepsilon_{xx}^0+M_{xx}^1\,\delta\varepsilon_{xx}^1+P_{xx}^1\,\delta\varepsilon_{xx}^2+N_{xx}^1\,\delta\varepsilon_{yy}^0+M_{yy}^1\,\delta\varepsilon_{yy}^1+P_{yy}^1\,\delta\varepsilon_{yy}^2\\ &+N_{xy}^1\,\delta\varepsilon_{xy}^0+M_{xy}^1\,\delta\varepsilon_{xy}^1+P_{xy}^1\,\delta\varepsilon_{xy}^2+Q_{yz}^1\,\delta\gamma_{yz}^0+Q_{xz}^1\,\delta\gamma_{xz}^0\end{aligned}\right]d\Omega\\ &+\int_\Omega\left[\bar N_{xx}^0\frac{\partial w_0}{\partial x}\frac{\partial\delta w_0}{\partial x}+\bar N_{yy}^0\frac{\partial w_0}{\partial y}\frac{\partial\delta w_0}{\partial y}+2\bar N_{xy}^0\frac{\partial w_0}{\partial x}\frac{\partial\delta w_0}{\partial y}\right]d\Omega=0\end{aligned} \tag{13}$$

The stress resultants N, M, P and Q of the FGSP are expressed by:

$$\begin{Bmatrix} N_{xx}^1 \\ N_{yy}^1 \\ N_{xy}^1 \end{Bmatrix} = \sum_{n=1}^{3} \int_{h_{n-1}}^{h_n} \begin{Bmatrix} \sigma_{xx} \\ \sigma_{yy} \\ \tau_{xy} \end{Bmatrix}^{(n)} dz, \quad \begin{Bmatrix} M_{xx}^1 \\ M_{yy}^1 \\ M_{xy}^1 \end{Bmatrix} = \sum_{n=1}^{3} \int_{h_{n-1}}^{h_n} \begin{Bmatrix} \sigma_{xx} \\ \sigma_{yy} \\ \tau_{xy} \end{Bmatrix}^{(n)} z\,dz \tag{14a}$$

$$\begin{Bmatrix} P_{xx}^1 \\ P_{yy}^1 \\ P_{xy}^1 \end{Bmatrix} = \sum_{n=1}^{3} \int_{h_{n-1}}^{h_n} \begin{Bmatrix} \sigma_{xx} \\ \sigma_{yy} \\ \tau_{xy} \end{Bmatrix}^{(n)} f(z)\,dz, \quad \begin{Bmatrix} Q_{xz}^1 \\ Q_{yz}^1 \end{Bmatrix} = \sum_{n=1}^{3} \int_{h_{n-1}}^{h_n} \begin{Bmatrix} \tau_{xz} \\ \tau_{yz} \end{Bmatrix}^{(n)} g(z)\,dz \tag{14b}$$

Where: h_n and h_{n-1} represent the z-coordinates of the top and bottom surfaces, respectively, of the nth layer.

By substituting equation. (8) into equation. (10) and subsequently substituting the obtained results into equation (14), the stress resultants of the FGSP can be related to the total strains by:

$$\begin{bmatrix} N_{xx}^1 \\ N_{yy}^1 \\ N_{xy}^1 \\ M_{xx}^1 \\ M_{yy}^1 \\ M_{xy}^1 \\ P_{xx}^1 \\ P_{yy}^1 \\ P_{xy}^1 \end{bmatrix} = \begin{bmatrix} A_{11} & A_{12} & 0 & B_{11} & B_{12} & 0 & Cs_{11} & Cs_{12} & 0 \\ A_{12} & A_{22} & 0 & B_{12} & B_{22} & 0 & Cs_{12} & Cs_{22} & 0 \\ 0 & 0 & A_{66} & 0 & 0 & B_{66} & 0 & 0 & Cs_{66} \\ B_{11} & B_{12} & 0 & D_{11} & D_{12} & 0 & F_{11} & F_{12} & 0 \\ B_{12} & B_{22} & 0 & D_{12} & D_{22} & 0 & F_{12} & F_{22} & 0 \\ 0 & 0 & B_{66} & 0 & 0 & D_{66} & 0 & 0 & F_{66} \\ Cs_{11} & Cs_{12} & 0 & F_{11} & F_{12} & 0 & H_{11} & H_{12} & 0 \\ Cs_{12} & Cs_{22} & 0 & F_{12} & F_{22} & 0 & H_{12} & H_{22} & 0 \\ 0 & 0 & Cs_{66} & 0 & 0 & F_{66} & 0 & 0 & H_{66} \end{bmatrix} \begin{bmatrix} \varepsilon_{xx}^0 \\ \varepsilon_{yy}^0 \\ \varepsilon_{xy}^0 \\ \varepsilon_{xx}^1 \\ \varepsilon_{yy}^1 \\ \varepsilon_{xy}^1 \\ \varepsilon_{xx}^2 \\ \varepsilon_{yy}^2 \\ \varepsilon_{xy}^2 \end{bmatrix} \tag{15a}$$

$$\begin{Bmatrix} Q_{xz}^1 \\ Q_{yz}^1 \end{Bmatrix} = \begin{bmatrix} G_{44} & 0 \\ 0 & G_{55} \end{bmatrix} \begin{Bmatrix} \gamma_{xz}^0 \\ \gamma_{yz}^0 \end{Bmatrix} \tag{15b}$$

Where: A_{ij}, B_{ij}, Cs_{ij} …etc. are the plate's stiffness parameters, defined as follows:

$$\begin{Bmatrix} A_{11} & B_{11} & D_{11} & Cs_{11} & F_{11} & H_{11} \\ A_{12} & B_{12} & D_{12} & Cs_{12} & F_{12} & H_{12} \\ A_{66} & B_{66} & D_{66} & Cs_{66} & F_{66} & H_{66} \end{Bmatrix} = \sum_{n=1}^{3} \int_{h_n-1}^{h_n} [1, z, z^2, f(z), z\,f(z), f^2(z)] \begin{Bmatrix} C_{11} \\ C_{12} \\ C_{66} \end{Bmatrix} dz \tag{16a}$$

$$(A_{22}, B_{22}, D_{22}, C_{22}, F_{22}, H_{22}) = (A_{11}, B_{11}, D_{11}, C_{11}, F_{11}, H_{11})$$

$$G_{44} = G_{55} = \sum_{n=1}^{3} \int_{h_n-1}^{h_n} C_{44} \left[g(z) \right]^2 dz \tag{16b}$$

By substituting equations (9a) and (9b) into equation (13), the following equations of equilibrium of the plate are obtained as follows:

$$
\begin{aligned}
&\delta u_0: && \frac{N_{xx}^1}{\partial x}+\frac{\partial N_{xy}^1}{\partial y}=0\\
&\delta v_0: && \frac{\partial N_{xx}^1}{\partial x}+\frac{\partial N_{yy}^1}{\partial y}=0\\
&\delta w_0: && \frac{\partial^2 M_{xx}^1}{\partial x^2}+2\frac{\partial^2 M_{xy}^1}{\partial x\partial y}+\frac{\partial^2 M_{yy}^1}{\partial y^2}+q+\bar{N}_{xx}^0\frac{\partial^2 w_0}{\partial x^2}+\bar{N}_{yy}^0\frac{\partial^2 w_0}{\partial y^2}+2\bar{N}_{xy}^0\frac{\partial^2 w_0}{\partial x\partial y}=0\\
&\delta\theta: && -K_1A\frac{\partial^2 P_x^1}{\partial x^2}-K_2B\frac{\partial^2 P_{yy}^1}{\partial y^2}-(K_1A+K_2B)\frac{\partial^2 P_{xy}^1}{\partial x\partial y}+K_1A\frac{\partial Q_{xz}^1}{\partial x}+K_2B\frac{\partial Q_{yz}^1}{\partial y}=0
\end{aligned}
\tag{17}
$$

Substituting equations (9) and (15) into equation (17), the governing equations of equilibrium of the FGSP are defined in terms of displacements (u_0, v_0, w_0, θ) as:

$$
\begin{aligned}
\delta u_0: \quad & A_{11}\frac{\partial^2 u_0^1}{\partial x^2}+A_{66}\frac{\partial^2 u_0^1}{\partial y^2}+(A_{12}+A_{66})\frac{\partial^2 v_0^1}{\partial x\partial y}-B_{11}\frac{\partial^3 w_0^1}{\partial x^3}-(B_{12}+2B_{66})\frac{\partial^3 w_0^1}{\partial x\partial y^2}\\
&+Cs_{11}K_1A\frac{\partial^3\theta_0^1}{\partial x^3}+(Cs_{12}K_2B+Cs_{66}(K_1A+K_2B))\frac{\partial^3\theta_0^1}{\partial x\partial y^2}=0
\end{aligned}
\tag{18a}
$$

$$
\begin{aligned}
\delta v_0: \quad & (A_{12}+A_{66})\frac{\partial^2 u_0^1}{\partial x\partial y}+A_{22}\frac{\partial^2 v_0^1}{\partial y^2}+A_{66}\frac{\partial^2 v_0^1}{\partial x^2}-B_{22}\frac{\partial^3 w_0^1}{\partial y^3}-(B_{12}+2B_{66})\frac{\partial^3 w_0^1}{\partial x^2\partial y}\\
&+Cs_{22}K_2B\frac{\partial^3\theta_0^1}{\partial y^3}+(Cs_{12}K_1A+Cs_{66}(K_1A+K_2B))\frac{\partial^3\theta_0^1}{\partial x^2\partial y}=0
\end{aligned}
\tag{18b}
$$

$$
\begin{aligned}
\delta w_0: \quad & B_{11}\frac{\partial^3 u_0^1}{\partial x^3}+(B_{12}+2B_{66})\frac{\partial^3 u_0^1}{\partial x\partial y^2}+B_{22}\frac{\partial^3 v_0^1}{\partial y^3}+(B_{12}+2B_{66})\frac{\partial^3 v_0^1}{\partial x^2\partial y}-D_{11}\frac{\partial^4 w_0^1}{\partial x^4}\\
&-D_{22}\frac{\partial^4 w_0^1}{\partial y^4}-2(D_{12}+2D_{66})\frac{\partial^4 w_0^1}{\partial x^2\partial y^2}+F_{11}K_1A\frac{\partial^4\theta_0^1}{\partial x^4}+F_{22}K_2B\frac{\partial^4\theta_0^1}{\partial y^4}+\\
&(F_{12}+2F_{66})(K_1A+K_2B)\frac{\partial^4\theta_0^1}{\partial x^2\partial y^2})+N_{xx}^0\frac{\partial^2 w_0^1}{\partial x^2}+\bar{N}_{yy}^0\frac{\partial^2 w_0^1}{\partial y^2}+2\bar{N}_{xy}^0\frac{\partial^2 w_0^1}{\partial x\partial y}=0
\end{aligned}
\tag{18c}
$$

$$
\begin{aligned}
\delta\theta: \quad & -Cs_{11}K_1A\frac{\partial^3 u_0^1}{\partial x^3}-(Cs_{12}K_2B+Cs_{66}(K_1A+K_2B)\frac{\partial^3 u_0^1}{\partial x\partial y^2}-Cs_{22}K_2B\frac{\partial^3 v_0^1}{\partial x^3}\\
&-(Cs_{12}K_1A+Cs_{66}(K_1A+K_2B))\frac{\partial^3 v_0^1}{\partial x^2\partial y}+F_{11}K_1A\frac{\partial^4 w_0^1}{\partial x^4}+F_{22}K_2B\frac{\partial^4 w_0^1}{\partial y^4}\\
&+(K_1A+K_2B)(F_{12}+2F_{66})\frac{\partial^4 w_0^1}{\partial x^2\partial y^2}-H_{11}(K_1A)^2\frac{\partial^4\theta_0^1}{\partial x^4}-H_{22}(K_2B)^2\frac{\partial^4\theta_0^1}{\partial y^4}\\
&-(2H_{12}K_1AK_2B+H_{66}(K_1A+K_2B)^2)\frac{\partial^4\theta_0^1}{\partial x^2\partial x^2}=0
\end{aligned}
\tag{18d}
$$

2.3. Exact solution for the FGSP under various boundary conditions

Here, we are interested in the analytical solutions of equations (17) for the FGSP under various boundary conditions can be constructed. A general solution of different boundary conditions is used to solve the governing equations based on the proposed theory. To this end, the displacement field can be considered as[22]:

$$\begin{Bmatrix} u_0^1 \\ v_0^1 \\ w_0^1 \\ \theta_0^1 \end{Bmatrix} = \sum_{m=1}^{\infty}\sum_{n=1}^{\infty} \begin{Bmatrix} U_{mn}\dfrac{\partial X_m(x)}{\partial x} Y_n(y) \\ V_{mn}\, X_m(x)\dfrac{\partial Y_n(y)}{\partial y} \\ W_{mn}\, X_m(x)\, Y_n(y) \\ X_{mn} X_m(x)\, Y_n(y) \end{Bmatrix} \tag{19}$$

Where: $\mathbf{U_{mn}}$, $\mathbf{V_{mn}}$, $\mathbf{W_{mn}}$, and $\mathbf{X_{mn}}$, are arbitrary parameters to be determined. The in-plane forces are given as follows:

$$\bar{N}_{xx}^0 = \gamma_1 N_{cr},\ \bar{N}_{yy}^0 = \gamma_2 N_{cr},\ \ \bar{N}_{xy}^0 = 0 \tag{20}$$

The parameter represents the direction of the in-plane forces.
By substituting equations. (19) and (20) into equation. (18), the obtained equations are:

$$\begin{bmatrix} L_{11} & L_{12} & L_{13} & L_{14} \\ L_{21} & L_{22} & L_{23} & L_{24} \\ L_{31} & L_{32} & L_{33}+\zeta & L_{34} \\ L_{41} & L_{42} & L_{43} & L_{44} \end{bmatrix} \begin{Bmatrix} U_{mn} \\ V_{mn} \\ W_{mn} \\ X_{mn} \end{Bmatrix} = \begin{Bmatrix} 0 \\ 0 \\ 0 \\ 0 \end{Bmatrix} \tag{21}$$

The elements Lij are expressed as follows:

$$\begin{aligned}
L_{11} &= A_{11}\alpha_{12} - A_{66}\alpha_8 \\
L_{12} &= (A_{12} + A_{66})\alpha_8 \\
L_{13} &= -B_{11}\alpha_{12} - (B_{12} + 2B_{66})\alpha_8 \\
L_{14} &= (Cs_{12}K_2B + Cs_{66}(K_1A + K_2B))\alpha_8 + Cs_{11}K_1A\alpha_{12} \\
L_{21} &= (A_{12} + A_{66})\alpha_{10} \\
L_{22} &= A_{11}\alpha_4 - A_{66}\alpha_{10} \\
L_{23} &= -B_{11}\alpha_4 - (B_{12} + 2B_{66})\alpha_{10} \\
L_{24} &= Cs_{22}K_2B\alpha_4 + (Cs_{12}K_1A + Cs_{66}(K_1A + K_2B))\alpha_{10} \\
L_{31} &= B_{11}\alpha_{13} + (B_{12} + 2B_{66})\alpha_{11} \\
L_{32} &= B_{11}\alpha_5 + (B_{12} + 2B_{66})\alpha_{11} \\
L_{33} &= -D_{11}\alpha_{13} - D_{22}\alpha_5 - 2(D_{12} + 2D_{66})\alpha_{11} \\
L_{34} &= F_{11}K_1A\alpha_{12} + (F_{12} + 2F_{66})(K_1A + K_2B))\alpha_{11} + F_{22}K_2B\alpha_5 \\
L_{41} &= -Cs_{11}K_1A\alpha_{13} - (Cs_{12}K_2B + Cs_{66}(K_1A + K_2B))\alpha_{11} \\
L_{42} &= -Cs_{22}K_2B\alpha_5 - (Cs_{12}K_1A + Cs_{66}(K_1A + K_2B))\alpha_{11} \\
L_{43} &= F_{11}K_1A\alpha_{13} + (F_{12} + 2F_{66})(K_1A + K_2B))\alpha_{11} + F_{22}K_2B\alpha_5 \\
L_{44} &= -(2H_{12}K_1AK_2B + H_{66}(K_1A + K_2B)^2)\alpha_{11} - H_{11}(K_1A)^2\alpha_{13} \\
&\quad - H_{22}(K_2B)^2\alpha_5 - G_{44}((K_1A)^2\alpha_9 + (K_2B)^2\alpha_3) \\
\zeta &= N_{cr}(\gamma_1\alpha_9 + \gamma_2\alpha_3)
\end{aligned} \tag{22}$$

With:

$$
\begin{aligned}
(\alpha_1,\alpha_3,\alpha_5) &= \int_0^a\int_0^b (X_mY_n, X_mY_n'', X_mY^{\text{""}})X_mY_n\,dx\,dy \\
(\alpha_2,\alpha_4,\alpha_{10}) &= \int_0^a\int_0^b (X_mY_n', X_mY_n''', X_m''Y_n')X_mY_n'\,dx\,dy \\
(\alpha_6,\alpha_8,\alpha_{12}) &= \int_0^a\int_0^b (X_m'Y_n', X_m'Y_n'', X_m'''Y_n)X_m'Y_n\,dx\,dy \\
(\alpha_7,\alpha_9,\alpha_{11},\alpha_{13}) &= \int_0^a\int_0^b (X_m'Y_n', X_m''Y_n, X_m''Y_n'', X_m''''Y_n)X_mY_n\,dx\,dy
\end{aligned}
\tag{23}
$$

3. Numerical results and discussion

This section presents and discusses multiple numerical examples of simply supported FGSPs. The goal is to validate the accuracy of the proposed theory in predicting the bending behavior by comparing the results with existing data in the literature. The FGSPs in these examples comprise Aluminum (Al) as the metal phase and Zirconia (ZrO2) as the ceramic phase. The mechanical properties of the FGSPs, including Young's modulus, Poisson's ratio, and density, are defined as follows[38, 39]

- Aluminum (Al): $E_m = 70Gpa,\ \nu_m = 0.3$ and $\rho_m = 2702\ kg/m^3$
- Zirconia (ZrO_2): $E_c = 380Gpa,\ \nu_c = 0.3$ and $\rho_c = 3100\ kg/m^3$

The results of the numerical analysis are expressed using non-dimensional stresses and deflection. The Dimensionless parameters utilized in this study are listed below:

$$N_{cr} = \frac{\bar{N}\,a^2}{100\,h^3E_0},$$

Where the reference value is taken as E_0 = 1 GPa

Table 1. Dimensionless buckling load N_{cr} of square plates under uniaxial compression ($\gamma_1 = -1,\ \gamma_2 = 0,\ a/h = 10$)

k	Theory	1-0-1	2-1-2	1-1-1	2-2-1	1-2-1
0	El Meiche et al[40]	13.0055	13.0055	13.0055	13.0055	13.0055
	Huu-Tai T et al.[36]	13.0045	13.0045	13.0045	13.0045	13.0045
	Meksi et al. [41]	13.0236	13.0236	13.0236	13.0236	13.0236
	Present	13.0051	13.0051	13.0051	13.0051	13.0051
0.5	El Meiche et al[40]	7.3638	7.9405	8.4365	8.8103	9.2176
	Huu-Tai T et al. [36]	7.3634	7.9403	8.4361	8.8095	9.2162
	Meksi et al. [41]	7.3664	7.9442	8.4423	8.8182	9.2277
	Present	7.3648	7.9412	8.4366	8.8100	9.2166
1	El Meiche et al[40]	5.1663	5.8394	6.4645	6.9495	7.5072
	Huu-Tai T et al.[36]	5.1648	5.8387	6.4641	6.9485	7.5056
	Meksi et al. [41]	5.1651	5.8392	6.4664	6.9536	7.5138
	Present	5.1676	5.8405	6.4649	6.9495	7.5063
5	El Meiche et al [40]	2.6568	3.0414	3.5787	4.1116	4.7346
	Huu-Tai T et al.[36]	2.6415	3.0282	3.5710	4.1024	4.7305
	Meksi et al. [41]	2.6518	3.0369	3.5756	4.1103	4.7351
	Present	2.6590	3.0408	3.5800	4.1124	4.7347
10	El Meiche et al[40]	2.4857	2.7450	3.1937	3.7069	4.2796
	Huu-Tai T et al.[36]	2.4666	2.7223	3.1795	3.6901	4.2728
	Meksi et al. [41]	2.4808	2.7397	3.1898	3.7048	4.2789
	Present	2.4881	2.7470	3.1952	3.7079	4.2800

Table 2. Dimensionless buckling load N_{cr} of square plates under biaxial compression ($\gamma 1 = -1$, $\gamma 2 = -1$, a/h = 10)

k	Theory	1-0-1	2-1-2	1-1-1	2-2-1	1-2-1
0	Huu-Tai T et al.[36]	6.5022	6.5022	6.5022	6.5022	6.5022
	Meksi et al. [41]	6.5118	6.5118	6.5118	6.5118	6.5118
	Daikh et al.[34]	6.5026	6.5026	6.5026	6.5026	6.5026
	Present	6.5026	6.5026	6.5026	6.5026	6.5026
0.5	Huu-Tai T et al.[36]	3.6817	3.9702	4.2181	4.4047	4.6081
	Meksi et al. [41]	3.6832	3.9721	4.2212	4.4091	4.6138
	Daikh et al. [34]	3.6825	3.9706	4.2183	4.4050	4.6083
	Present	3.6824	3.9706	4.2183	4.4050	4.6083
1	Huu-Tai T et al.[36]	2.5824	2.9193	3.2320	3.4742	3.7528
	Meksi et al. [41]	2.5826	2.9196	3.2332	3.4768	3.7569
	Daikh et al. [34]	2.5839	2.9203	3.2325	3.4748	3.7531
	Present	2.5838	2.9202	3.2325	3.4748	3.7532
5	Huu-Tai T et al. [36]	1.3208	1.5141	1.7855	2.0512	2.3652
	Meksi et al. [41]	1.3259	1.5185	1.7878	2.0551	2.3676
	Daikh et al. [34]	1.3296	1.5216	1.7900	2.0562	2.3673
	Present	1.3295	1.5216	1.7900	2.0562	2.3673
10	Huu-Tai T et al.[36]	1.2333	1.3612	1.5897	1.8450	2.1364
	Meksi et al. [41]	1.2404	1.3699	1.5949	1.8524	2.1395
	Present	1.2441	1.3735	1.5976	1.8539	2.1400

Tables 1 and 2 present the non-dimensional values of the critical buckling load, N_{cr}, for various types of simply supported sandwich square plates under uniaxial and biaxial compression, respectively, and different values of index k. The results obtained from the present theory are compared with those presented by Meiche et al. [40], Huu-Tai Thai et al. [36], Daikh et al. [34], and Meksi et al. [41]. It is to be noted that the critical buckling decreases with increasing index k. Furthermore, the present hyperbolic shear deformation theory (HPT) gives a very good accuracy.

Table 3. Dimensionless buckling load N_{cr} of square plates under Various Boundary Conditions ($\gamma_1 = -1$, $\gamma_2 = -1$, $a/h = 10$).

Boundary conditions	Theory	k	1-0-1	2-1-2	1-1-1	2-2-1	1-2-1
SSSS	Huu-Tai T et al. [36]	0.5	3.6817	3.9702	4.2181	4.4047	4.6081
		1	2.5824	2.9193	3.2320	3.4742	3.7528
	Present	0.5	3.6824	3.9706	4.2183	4.4050	4.6083
		1	2.5838	2.9202	3.2325	3.4748	3.7532
CSCS	Huu-Tai T et al. [36]	0.5	6.8587	7.3942	7.8489	8.1861	8.5573
		1	4.8390	5.4712	6.0504	6.4925	7.0048
	Present	0.5	6.8613	7.3960	7.8500	8.1872	8.5583
		1	4.8441	5.4744	6.0520	6.4944	7.0063
CCCC	Huu-Tai T et al. [36]	0.5	9.2338	9.9529	10.5578	11.0011	11.4933
		1	6.5434	7.3990	8.1753	8.7612	9.4443
	Present	0.5	9.2438	9.9618	10.566	11.010	11.5018
		1	6.5565	7.4091	8.1830	8.7697	9.4524
FCFC	Huu-Tai T et al. [36]	0.5	10.8640	11.7085	12.4145	12.9276	13.5006
		1	7.7220	8.7323	9.6429	10.3246	11.1229
	Present	0.5	10.8712	11.7137	12.4180	12.9315	13.5042
		1	7.7353	8.7409	9.6475	10.3300	11.1273

Table 3 illustrates the effect of various boundary conditions, different schemes of sandwich configuration, and index k on the critical buckling load, Ncr, of the FGM sandwich plate under a biaxial compression load with (γ1=-1, γ2=-1, a/h=10). It can be noted that the configuration 1-2-1 with FCFC has the highest critical buckling load values. Furthermore, it has been noted that the current results agree well with those obtained by Huu-Tai T et al. [36].

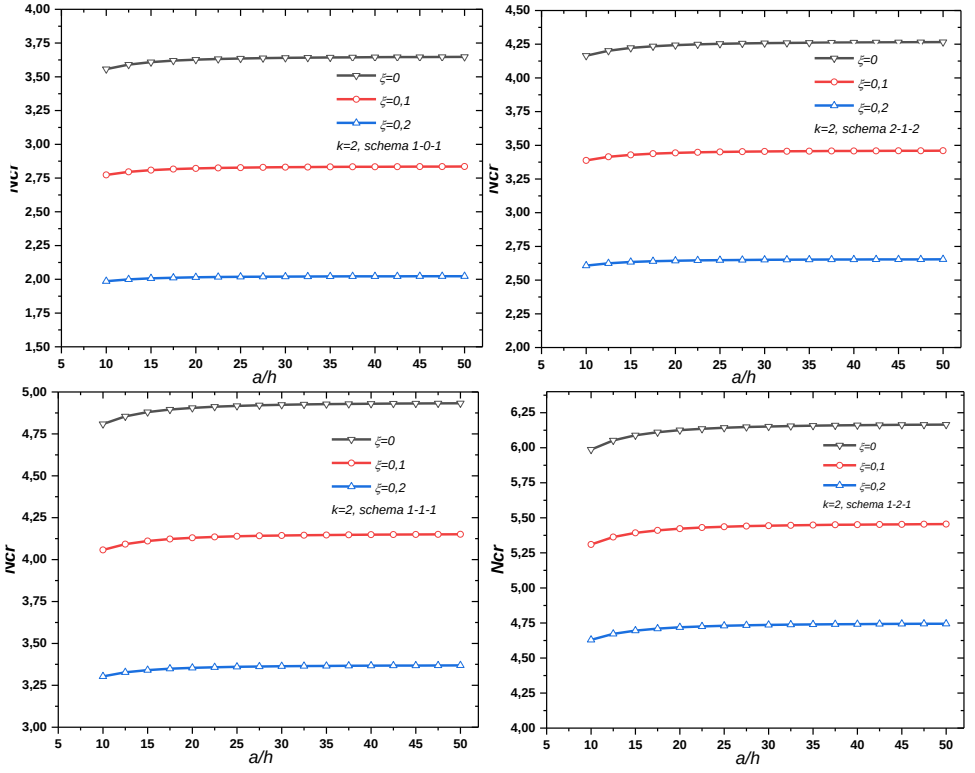

Fig 2.a Critical buckling load N_{cr} versus the ratio *a/h* for the different values of porosity coefficient of simply supported FGM sandwich square plates under uniaxial compression.

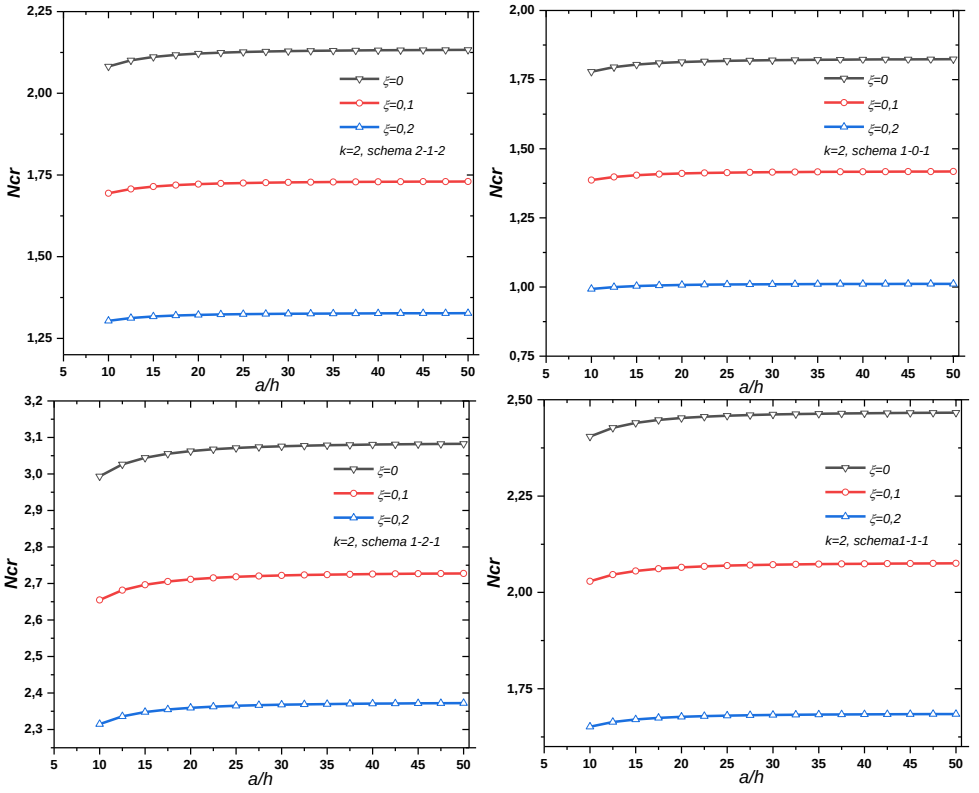

Figure 2.b Critical buckling load N_{cr} versus the ratio a/h for the different values of porosity coefficient of simply supported FGM sandwich square plates under bi-axial compression.

Figures 2.a and 2.b show the impact of the side-to-thickness ratio and the porosity distribution on the critical buckling load N_{cr} of the FG sandwich plate (2-1-2, 1-0-1, 1-2-1 and 1-1-1), k = 2. It can be seen that the critical buckling increases with increasing a/h when the inclusion of porosity reduces the critical buckling; this is because of the porosity coefficient's effect on the plate's stiffness.

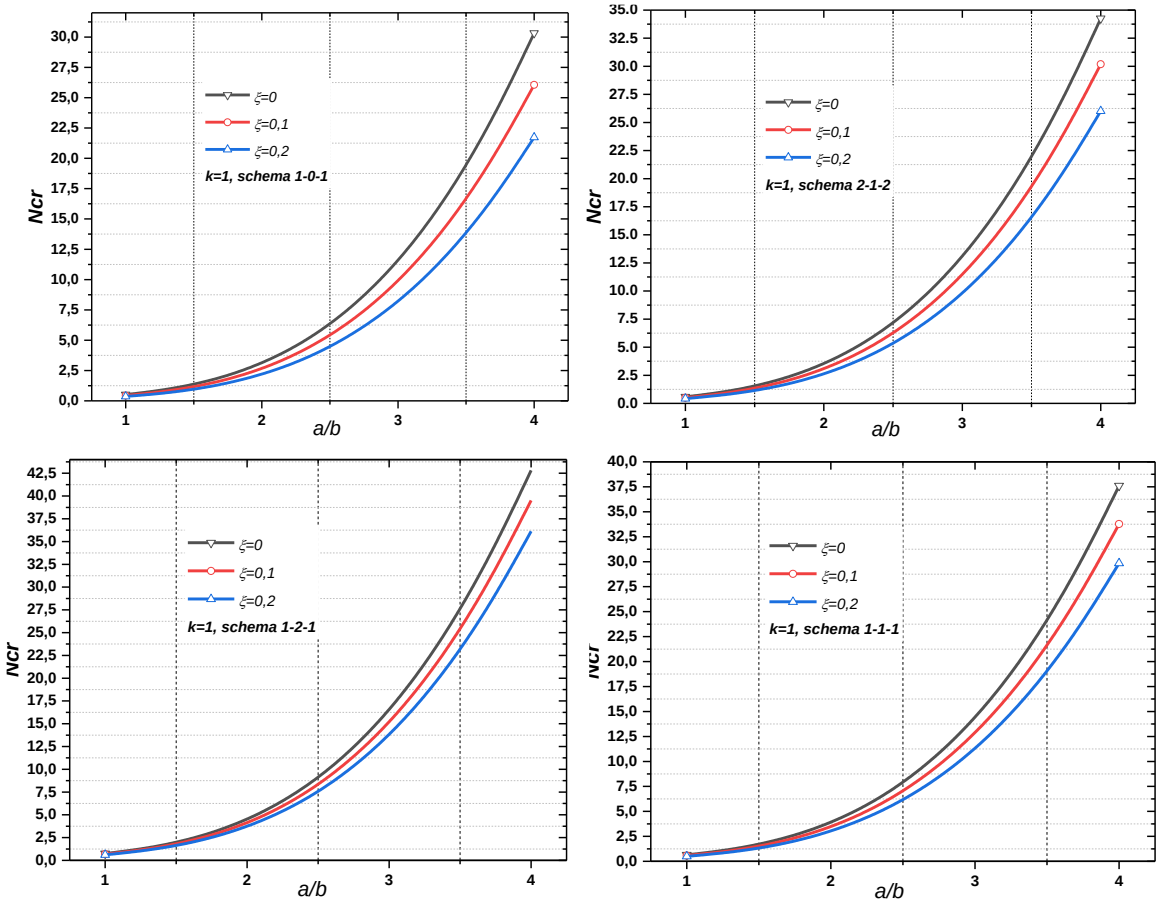

Figure 3.a Critical buckling load N_{cr} versus the ratio *a/b* for the different values of porosity coefficient of simply supported FGM sandwich plates under uniaxial compression.

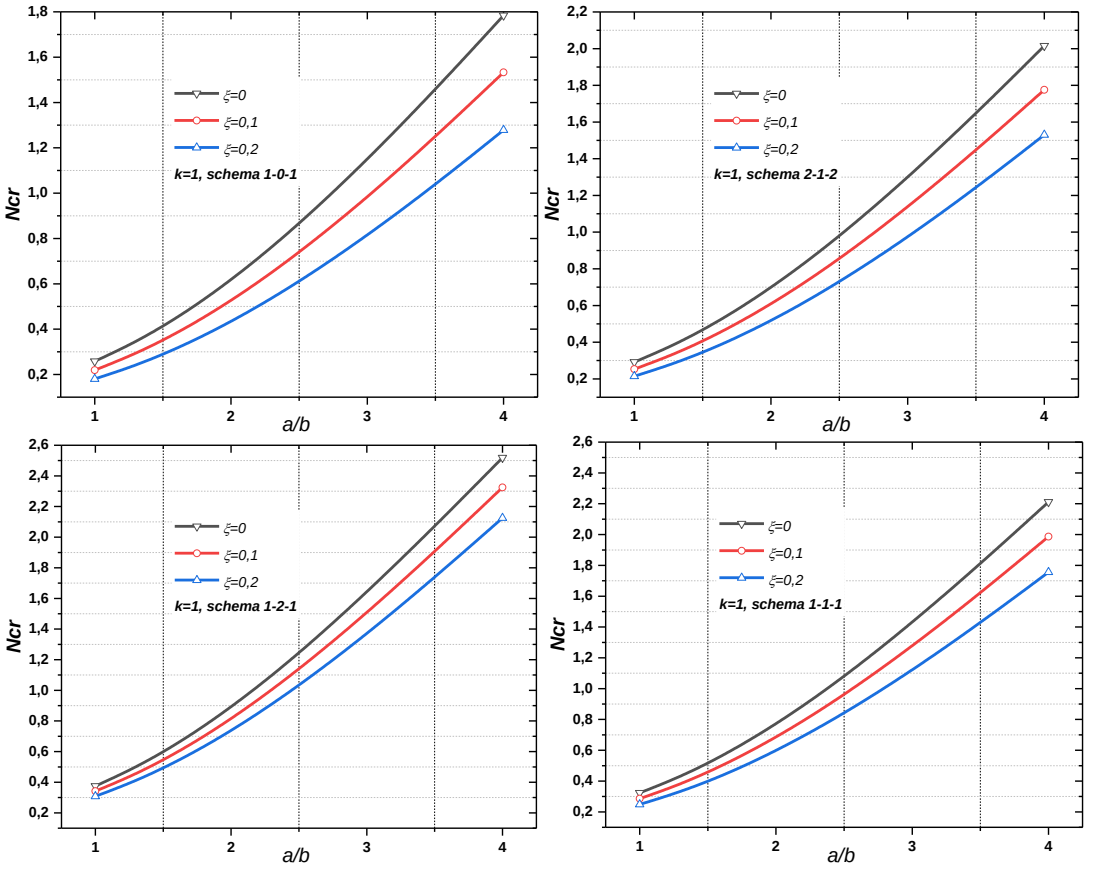

Figure 3.b Critical buckling load N_{cr} versus the ratio *a/b* for the different values of porosity coefficient of simply supported FGM sandwich plates under bi-axial compression.

Figures 3.a and 3.b depict the variation of the critical buckling load versus the aspect ratio a/b for the FG sandwich plate under uniaxial and bi-axial load with various values of porosity coefficient. It is observed that the increase of the aspect ratio increases the critical buckling load; however, the increase in the porosity coefficient decreases the critical buckling.

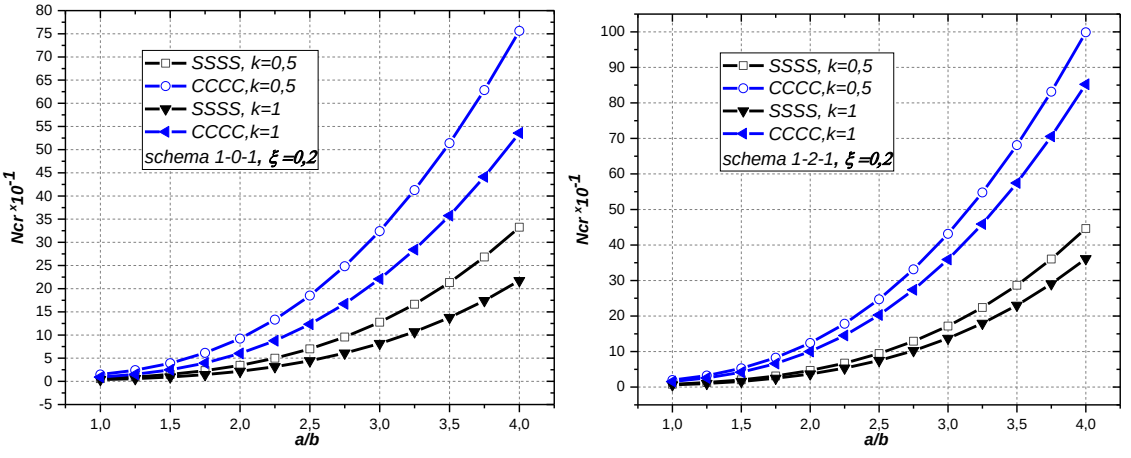

Figure 4. Critical buckling load N_{cr} versus the ratio *a/b* of the (1–2-1)/ (1–0–1) porous square FGM sandwich plates with various boundary conditions under uniaxial loads

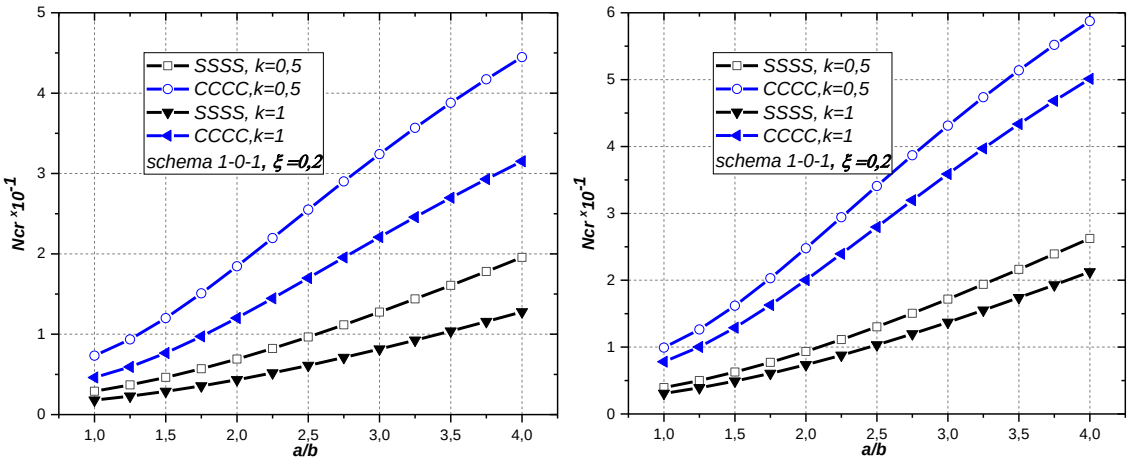

Figure 5. Critical buckling load N_{cr} versus the ratio *a/b* of the (1–2-1)/ (1–0–1) porous square FGM sandwich plates with various boundary conditions under bi-axial loads

Figure 4 presents the variation of the Critical buckling load Ncr of FG plates with ratio a/b resting on different boundary conditions under uniaxial compression loads. The plate with a higher volume fraction of ceramics has a significantly higher Critical buckling load Ncr than the plate with a higher metal volume fraction, particularly for plates with a larger a/b aspect ratio. Notably, the plate with all edges clamped boundary condition shows the highest non-dimensional Critical buckling load, owing to the more significant constraint at the edges, as depicted in **Figure 5**.

4. Conclusion

This study aims to analyze the effect of the different porosity sizes and various boundary conditions on the stiffness of the sandwich plate made on functionally graded materials under axial and bi-axial mechanical loading. So, an efficient higher-order theory is proposed for analyzing the buckling response of functionally graded sandwich plates; the mathematical formulation, including the indeterminate integral terms in the displacement field, and the governing equations are obtained by Hamilton's principle. The study presents analytical solutions with different boundary conditions. It provides numerical results to validate the accuracy of the proposed theory.

The following conclusions from the numerical computations are given as follows:

- The findings reveal that the buckling load for fully clamped-free-clamped-free boundary conditions is higher than other boundary conditions, including simply supported-simply supported, clamped-clamped, and clamped-simply supported.
- The 1-2-1 type sandwich has the highest critical buckling load, while the 2-1-2 type has the lowest.
- The results also suggest that the side-to-thickness ratio's effect on the critical buckling load of FGM sandwich plates diminishes for larger ratio values.
- Finally, the study shows that increasing the porosity coefficient reduces the critical buckling load values.

References

[1] J. Jamali, M. Naei, F. Honarvar, M. Rajabi, Acoustic scattering from functionally graded cylindrical shells, *Archives of Mechanics,* Vol. 63, No. 1, pp. 25-56, 2011.

[2] O. Taleb, M. Sekkal, R. B. Bouiadjra, S. Benyoucef, K. M. Khedher, M. A. Salem, A. Tounsi, On the Free Vibration Behavior of Temperature-Dependent Bidirectional Functionally Graded Curved Porous Beams, *International Journal of Structural Stability and Dynamics*, pp. 2450112, 2023.

[3] H. Z. Guerroudj, R. Yeghnem, A. Kaci, F. Z. Zaoui, S. Benyoucef, A. Tounsi, Eigenfrequencies of advanced composite plates using an efficient hybrid quasi-3D shear deformation theory, *Smart structures and systems*, Vol. 22, No. 1, pp. 121-132, 2018.

[4] A. Edwin, V. Anand, K. Prasanna, Sustainable development through functionally graded materials: an overview, *Rasayan Journal of Chemistry*, Vol. 10, No. 1, pp. 149-152, 2017.

[5] G. Udupa, S. S. Rao, K. Gangadharan, Functionally graded composite materials: an overview, *Procedia Materials Science,* Vol. 5, pp. 1291-1299, 2014.

[6] H.-T. Thai, B. Uy, M. Khan, Z. Tao, F. Mashiri, Numerical modelling of concrete-filled steel box columns incorporating high strength materials, *Journal of Constructional Steel Research*, Vol. 102, pp. 256-265, 2014.

[7] S.-H. Chi, Y.-L. Chung, Mechanical behavior of functionally graded material plates under transverse load—Part I: Analysis, *International Journal of Solids and Structures,* Vol. 43, No. 13, pp. 3657-3674, 2006.

[8] R. Javaheri, M. Eslami, Buckling of functionally graded plates under in-plane compressive loading, *ZAMM-Journal of Applied Mathematics and Mechanics/Zeitschrift für Angewandte Mathematik und Mechanik: Applied Mathematics and Mechanics*, Vol. 82, No. 4, pp. 277-283, 2002.

[9] E. Feldman, J. Aboudi, Buckling analysis of functionally graded plates subjected to uniaxial loading, *Composite Structures,* Vol. 38, No. 1-4, pp. 29-36, 1997.

[10] R. Menaa, A. Tounsi, F. Mouaici, I. Mechab, M. Zidi, E. A. A. Bedia, Analytical solutions for static shear correction factor of functionally graded rectangular beams, *Mechanics of Advanced Materials and Structures,* Vol. 19, No. 8, pp. 641-652, 2012.

[11] M. Rashidi, A. Shooshtari, O. A. Bég, Homotopy perturbation study of nonlinear vibration of Von Karman rectangular plates, *Computers & Structures,* Vol. 106, pp. 46-55, 2012.

[12] R. Mindlin, Influence of rotatory inertia and shear on flexural motions of isotropic, elastic plates, 1951.

[13] E. Reissner, The effect of transverse shear deformation on the bending of elastic plates, 1945.

[14] A. Bouhadra, A. Tounsi, A. A. Bousahla, S. Benyoucef, S. R. Mahmoud, Improved HSDT accounting for effect of thickness stretching in advanced composite plates, *Structural Engineering and Mechanics, An Int'l Journal*, Vol. 66, No. 1, pp. 61-73, 2018.

[15] D. Chen, J. Yang, S. Kitipornchai, Buckling and bending analyses of a novel functionally graded porous plate using Chebyshev-Ritz method, *Archives of Civil and Mechanical Engineering*, Vol. 19, No. 1, pp. 157-170, 2019.

[16] J. Reddy, C. Wang, S. Kitipornchai, Axisymmetric bending of functionally graded circular and annular plates, *European Journal of Mechanics-A/Solids*, Vol. 18, No. 2, pp. 185-199, 1999.

[17] M. Mekerbi, R. Bachir Bouiadjra, S. Benyoucef, M. Selim, A. Tounsi, M. Hussain, Micromechanical models for analyzing bending of porous/perfect FG plates in a hygro-thermomechanical environment by a quasi-3D theory, *Mechanics of Composite Materials,* Vol. 59, No. 4, pp. 693-712, 2023.

[18] F. Achouri, S. Benyoucef, F. Bourada, R. B. Bouiadjra, A. Tounsi, Robust quasi 3D computational model for mechanical response of FG thick sandwich plate, *Struct. Eng. Mech*, Vol. 70, No. 5, pp. 571-589, 2019.

[19] S. Moradi, M. H. Mansouri, Thermal buckling analysis of shear deformable laminated orthotopic plates by differential quadrature, *Steel & Composite Structures,* Vol. 12, No. 2, pp. 129-147, 2012.

[20] A. Kabouche, R. Bachir Bouiadjra, A. Bachiri, M. Sekkal, S. Benyoucef, M. M. S. Saleh, A. Tounsi, M. Hussain, Study on the Mechanical Instability of Bidirectional Imperfect FG Sandwich Plates Subjected to In-Plane Loading, *Arabian Journal for Science and Engineering*, Vol. 47, No. 10, pp. 13655-13672, 2022.

[21] X. Zhao, Y. Lee, K. M. Liew, Mechanical and thermal buckling analysis of functionally graded plates, *Composite Structures*, Vol. 90, No. 2, pp. 161-171, 2009.

[22] M. Mekerbi, S. Benyoucef, A. Mahmoudi, F. Bourada, A. Tounsi, Investigation on thermal buckling of porous FG plate resting on elastic foundation via quasi 3D solution, *Structural Engineering and Mechanics,* Vol. 72, No. 4, pp. 513, 2019.

[23] A. Chikh, A. Tounsi, H. Hebali, S. Mahmoud, Thermal buckling analysis of cross-ply laminated plates using a simplified HSDT, *Smart Structures and Systems,* Vol. 19, No. 3, pp. 289-297, 2017.

[24] A. Tamrabet, B. Mamen, A. Menasria, A. Bouhadra, A. Tounsi, M. H. Ghazwani, A. Alnujaie, S. Mahmoud, Buckling behaviors of FG porous sandwich plates with metallic foam cores resting on elastic foundation, *Structural Engineering and Mechanics*, Vol. 85, No. 3, pp. 289, 2023.

[25] D. Chen, J. Yang, S. Kitipornchai, Nonlinear vibration and postbuckling of functionally graded graphene reinforced porous nanocomposite beams, *Composites Science and Technology*, Vol. 142, pp. 235-245, 2017.

[26] D. Chen, J. Yang, S. Kitipornchai, Free and forced vibrations of shear deformable functionally graded porous beams, *International journal of mechanical sciences*, Vol. 108, pp. 14-22, 2016.

[27] A. Meksi, M. Sekkal, R. B. Bouiadjra, S. Benyoucef, A. Tounsi, Assessing the effect of temperature-dependent properties on the dynamic behavior of FG porous beams rested on variable elastic foundation, *Structural Engineering and Mechanics*, Vol. 85, No. 6, pp. 717, 2023.

[28] R. B. Bouiadjra, A. Mahmoudi, M. Sekkal, S. Benyoucef, M. M. Selim, A. Tounsi, M. Hussain, A quasi 3D solution for thermodynamic response of FG sandwich plates lying on variable elastic foundation with arbitrary boundary conditions, *Steel and Composite Structures, An International Journal*, Vol. 41, No. 6, pp. 873-886, 2021.

[29] M. Mekerbi, S. Benyoucef, A. Mahmoudi, A. Tounsi, A. A. Bousahla, S. Mahmoud, Thermodynamic behavior of functionally graded sandwich plates resting on different elastic foundation and with various boundary conditions, *Journal of Sandwich Structures & Materials*, Vol. 23, No. 3, pp. 1028-1057, 2021.

[30] Ö. Civalek, Geometrically nonlinear dynamic analysis of doubly curved isotropic shells resting on elastic foundation by a combination of harmonic differential quadrature-finite difference methods, *International Journal of Pressure Vessels and Piping*, Vol. 82, No. 6, pp. 470-479, 2005.

[31] E. Sobhani, A. Arbabian, Ö. Civalek, M. Avcar, The free vibration analysis of hybrid porous nanocomposite joined hemispherical–cylindrical–conical shells, *Engineering with Computers*, pp. 1-28, 2021.

[32] S. Dastjerdi, B. Akgöz, Ö. Civalek, M. Malikan, V. A. Eremeyev, On the non-linear dynamics of torus-shaped and cylindrical shell structures, *International Journal of Engineering Science*, Vol. 156, pp. 103371, 2020.

[33] M. Chitour, S. Benguediab, A. Bouhadra, F. Bourada, M. Benguediab, A. Tounsi, Effect of variable volume fraction distribution and geometrical parameters on the bending behavior of sandwich plates with FG isotropic face sheets, *Mechanics Based Design of Structures and Machines*, pp. 1-27, 2023.

[34] A. A. Daikh, A. M. Zenkour, Free vibration and buckling of porous power-law and sigmoid functionally graded sandwich plates using a simple higher-order shear deformation theory, *Materials Research Express*, Vol. 6, No. 11, pp. 115707, 2019.

[35] M. Chitour, A. Bouhadra, M. Benguediab, K. Mansouri, A. Menasria, A. Tounsi, A New High Order Theory for Buckling Temperature Analysis of Functionally Graded Sandwich Plates Resting on Elastic Foundations, *Journal of Nano-and Electronic Physics*, Vol. 14, No. 3, 2022.

[36] H.-T. Thai, T.-K. Nguyen, T. P. Vo, J. Lee, Analysis of functionally graded sandwich plates using a new first-order shear deformation theory, *European Journal of Mechanics-A/Solids*, Vol. 45, pp. 211-225, 2014.

[37] B. M. N.Himeur, S. Benguediab, A. Bouhadra, A.Menasria, B. Bouchouicha, F. Bourada, M. Benguediab and A. Tounsi, *Steel Compost. Struct*, Vol. 44, 339-355. , 2022.

[38] A. Berkia, M. Benguediab, A. Bouhadra, K. Mansouri, A. Tounsi, M. Chitour, Influence of Mechanical and Geometric Characteristics on Thermal Buckling of Functionally Graded Sandwich Plates, *Journal of Nano- and Electronic Physics*, Vol. 14, No. 3, 2022.

[39] A. Berkia, S. Benguediab, A. Menasria, A. Bouhadra, F. B. B. Mamen, A. Tounsi, K. H. Benrahou, M. Benguediab, M. Hussain, Static buckling analysis of bi-directional functionally graded sandwich (BFGSW) beams with two different boundary conditions, *Steel and Composite Structures*, Vol. 44, No. 4, pp. 503, 2022.

[40] N. El Meiche, A. Tounsi, N. Ziane, I. Mechab, A new hyperbolic shear deformation theory for buckling and vibration of functionally graded sandwich plate, *International Journal of Mechanical Sciences*, Vol. 53, No. 4, pp. 237-247, 2011.

[41] R. Meksi, S. Benyoucef, A. Mahmoudi, A. Tounsi, E. A. Adda Bedia, S. Mahmoud, An analytical solution for bending, buckling and vibration responses of FGM sandwich plates, *Journal of Sandwich Structures & Materials*, Vol. 21, No. 2, pp. 727-757, 2019.